Natural Resources Canada
Ressources naturelles Canada

Insights into the tectonothermal history of Melville Peninsula, Nunavut, provided by in situ SHRIMP geochronology and thermobarometry

R.G. Berman, W.J. Davis, D. Corrigan, and L. Nadeau

Geological Survey of Canada
Current Research 2015-4

2015

Canada

Geological Survey of Canada
Current Research 2015-4

Insights into the tectonothermal history of Melville Peninsula, Nunavut, provided by in situ SHRIMP geochronology and thermobarometry

R.G. Berman, W.J. Davis, D. Corrigan, and L. Nadeau

2015

ISSN 1701-4387
Catalogue No. M44-2015/4E-PDF
ISBN 978-1-100-25631-3
doi:10.4095/295852

A copy of this publication is also available for reference in depository libraries across Canada through access to the Depository Services Program's Web site at http://dsp-psd.pwgsc.gc.ca

This publication is available for free download through GEOSCAN
http://geoscan.ess.nrcan.gc.ca

Recommended citation

Berman, R.G., Davis, W.J., Corrigan, D., and Nadeau, L., 2015. Insights into the tectonothermal history of Melville Peninsula, Nunavut, provided by in situ SHRIMP geochronology and thermobarometry; Geological Survey of Canada, Current Research 2015-4, 18 p. doi:10.4095/295852

Critical review

S. Pehrsson

Authors

R.G. Berman (Rob.Berman@NRCan-RNCan.gc.ca)
W.J. Davis (Bill.Davis@NRCan-RNCan.gc.ca)
D. Corrigan (David.Corrigan@NRCan-RNCan.gc.ca)
Geological Survey of Canada
601 Booth Street
Ottawa, Ontario K1A 0E9

L. Nadeau (Leo.Nadeau@RNCan-NRCan.gc.ca)
Geological Survey of Canada
490, rue de la Couronne
Québec, Quebec G1K 9A9

Correction date:

Insights into the tectonothermal history of Melville Peninsula, Nunavut, provided by in situ SHRIMP geochronology and thermobarometry

R.G. Berman, W.J. Davis, D. Corrigan, and L. Nadeau

Berman, R.G., Davis, W.J., Corrigan, D., and Nadeau, L., 2015. Insights into the tectonothermal history of Melville Peninsula, Nunavut, provided by in situ SHRIMP geochronology and thermobarometry; Geological Survey of Canada, Current Research 2015-4, 18 p. doi:10.4095/295852

Abstract: Thermobarometric and in situ SHRIMP monazite geochronology indicate that two distinct metamorphic and deformational events affected Melville Peninsula. Monazite inclusions in garnet from two samples yielded ages of 2546 ± 7 Ma and 2539 ± 8 Ma. Textural features suggest they date an early deformation event in the development the Arrowsmith Orogen. Four samples from southern Melville Peninsula record monazite growth between ca. 1860 Ma and ca. 1820 Ma. Textures suggest that 1863 ± 6 Ma metamorphism initiated prior to pervasive regional deformation. Monazite growth is interpreted to date syntectonic garnet growth at ca. 1840 Ma and syntectonic, peak metamorphism at 1829 ± 4 Ma to 1825 ± 4 Ma. Petrological calculations define a clockwise P-T-t path consistent with crustal thickening that is attributed to ca. 1870 Ma collision of the Rae Craton with Meta Incognita microcontinent. Samples on northern Melville Peninsula record younger (ca. 1815–1767 Ma) monazite ages, potentially related to east-west compression that affected much of the central Rae Craton at this time.

Résumé : Les résultats d'une étude thermobarométrique combinés à ceux d'une étude géochronologique sur monazite effectuée *in situ* à la microsonde SHRIMP indiquent que deux épisodes distincts de métamorphisme et de déformation ont touché la presqu'île Melville. Des inclusions de monazite dans le grenat de deux échantillons ont livré des âges de 2546 ± 7 Ma et de 2539 ± 8 Ma. D'après les caractéristiques texturales, ils permettraient de dater les phases précoces de la déformation liée à la formation de l'orogène d'Arrowsmith. Quatre échantillons prélevés dans la partie sud de la presqu'île Melville témoignent d'une croissance de la monazite entre environ 1860 Ma et environ 1820 Ma. Les textures indiquent que le métamorphisme remontant à 1863 ± 6 Ma a commencé avant la déformation régionale aux effets généralisés. Selon notre interprétation, la croissance de la monazite permettrait de situer la croissance syntectonique du grenat à environ 1840 Ma et le pic du métamorphisme syntectonique, de 1829 ± 4 Ma à 1825 ± 4 Ma. Les calculs pétrologiques définissent un chemin P-T-t dans le sens horaire, cohérent avec un épaississement de la croûte qui est attribué à la collision du craton de Rae avec le microcontinent Meta Incognita survenue à environ 1870 Ma. Des échantillons prélevés dans la partie nord de la presqu'île Melville indiquent des âges sur monazite plus récents (env. 1815-1767 Ma), qui seraient peut-être liés à une compression est-ouest qui a touché une grande partie du centre du craton de Rae à cette époque.

INTRODUCTION

It has been well established from early studies of the Penrhyn Group that southern Melville Peninsula experienced Paleoproterozoic deformation and metamorphism (Henderson, 1983), but the precise timing has not been defined nor has the geographic extent of Paleoproterozoic events on northern Melville Peninsula been documented. Metamorphic studies initiated as part of the Melville Peninsula Integrated Geoscience project (Geo-Mapping for Energy and Minerals Program) help constrain tectonic and regional metallogenic models upon which exploration strategies for diamonds and precious- and base-metals in the area can be based. This report summarizes recently acquired constraints on the pressure, temperature, and timing (P-T-t) of multiple metamorphic and deformation events on Melville Peninsula.

REGIONAL GEOLOGICAL SETTING

Located in the north-central Rae Craton on the west side of Hudson Bay (Fig. 1), Melville Peninsula exposes Meso- to Neoarchean crust that, based on studies to the west and south, were variably reactivated during the Neoarchean and Paleoproterozoic (Berman et al., 2005; 2010a; 2013a, b; Berman, 2010). Melville Peninsula has been divided into four lithotectonic domains, consisting of, from north to south (Fig. 2; Corrigan et al., 2013), 1) a northern block consisting of granulite-facies orthogneiss and plutonic rocks with minor supracrustal screens; 2) the Prince Albert Block, which consists of upper-greenschist to middle-amphibolite facies Archean supracrustal rocks as well as plutonic rocks and orthogneiss; 3) variably deformed and metamorphosed metasedimentary rocks of the Paleoproterozoic Penrhyn Group that overlay and are in stratigraphic and/or thrust contact with the Prince Albert Block, and 4) the Repulse Bay Block, a predominantly gneissic domain composed of variably strained, high metamorphic grade orthogneiss intruded by charnockite and overlain by sparse belts of presumed Paleoproterozoic cover rocks. The boundary between the Prince Albert and Repulse Bay blocks, referred to as the Lyon Inlet boundary zone, consists of a steeply dipping zone of strong transposition that accommodated dextral transpressional shear (Spratt et al., 2013; Ganderton, 2013).

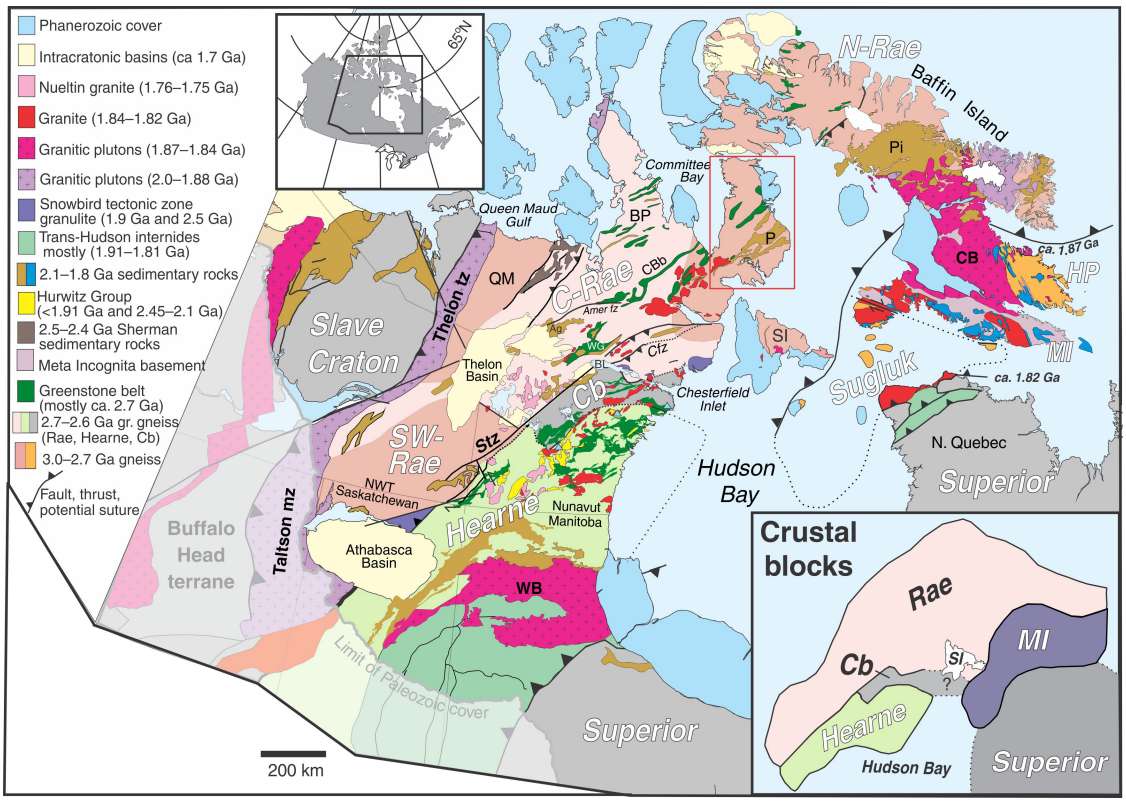

Figure 1. Regional geology of the Precambrian core of Laurentia flanking Hudson Bay, *modified from* Berman et al. (2005, 2013b). Ag = Amer group, BL = Baker Lake, BP = Boothia Peninsula, CBb = Committee Bay belt, Cb = Chesterfield Block, CB = Cumberland batholith, Cfz = Chesterfield fault zone, HP = Hall Peninsula, MI = Meta Incognita microcontinent, P = Penrhyn group, Pi = Piling Group, QM = Queen Maud Block, Rae = Rae Craton, SI = Southampton Island, Stz = Snowbird tectonic zone, WB = Wathaman batholith, fz = fault zone, tz = tectonic zone, mz = magmatic zone, WG = Woodburn Group. Red box shows location of Melville Peninsula illustrated in Figure 2.

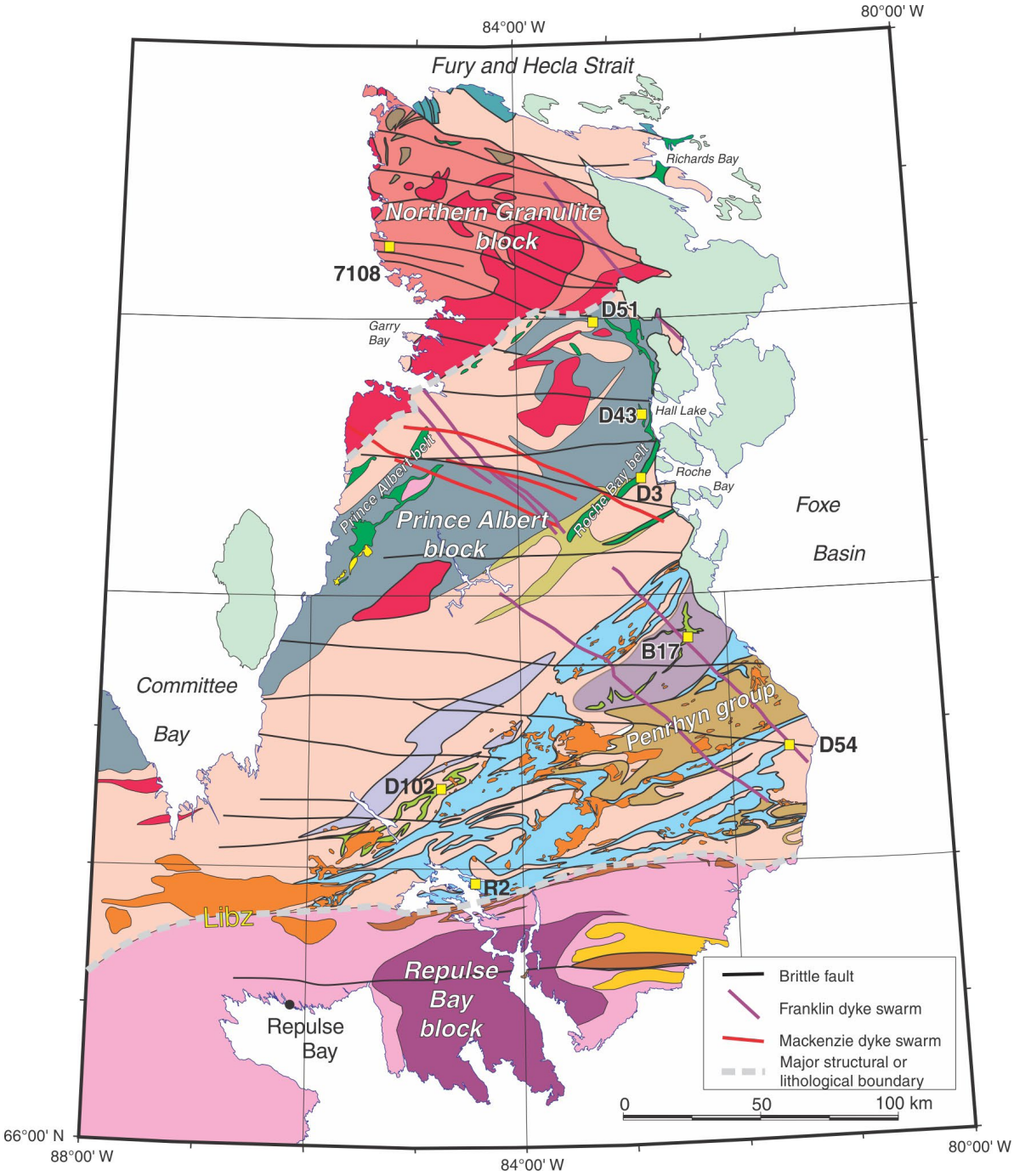

Figure 2. Simplified geology of Melville Peninsula (Corrigan et al., 2013). Yellow boxes show sample locations with abbreviated sample numbers.

Figure 2. (Legend)

A number of east- to east-southeast-striking brittle faults transect the peninsula (Fig. 2), both predating and postdating the Paleozoic cover sequence.

QUANTITATIVE METAMORPHIC AND GEOCHRONOLOGICAL CONSTRAINTS

Pressure-temperature conditions were estimated using the winTWQ software (version 2.35; Berman, 2007) following the methodology summarized by Berman et al. (2005). Unless otherwise described in the text, chemical variations in Fe/(Fe+Mg) of biotite and cordierite, and X_{An} of plagioclase are less than 2%, and pressure-temperature values were calculated from nearby rim compositions of ferromagnesian minerals (garnet, biotite) separated by quartz and/or plagioclase. In order to link pressure-temperature conditions to timing constraints, six metasedimentary rock samples were chosen that contained monazite of a size (>10 μm) suitable for in situ SHRIMP analysis, carried out on 3 mm diameter cores drilled from texturally significant areas of polished thin sections with the methods of Rayner and Stern (2002). A small plug of prepolished laboratory standard monazite (GSC monazite z3345 and z2908) was included on the mount. Stern and Berman (2001) described further analytical details. A Pb fractionation correction was applied to the Pb-isotope data in some instances, the magnitude of which was determined by analysis of monazite standards z3345 and z2908, the $^{207}Pb/^{206}Pb$ ages of which have been determined by isotope dilution methods (Stern and Berman, 2001). Errors in mass fractionation have been added quadratically to 2σ errors of weighted mean ages reported in the text. Common Pb correction utilized the Pb composition of the surface blank (Stern, 1997).

Table 1 summarizes thermobarometric and geochronological results for eight widely distributed samples (Fig. 2). Table 2 provides SHRIMP analytical data for monazite.

Table 1. Summary of age and pressure-temperature results.

Sample	Monazite texture	Age (Ma)	P (kbar)	T(°C)
Archean metamorphism and deformation at 2.54 Ga				
10CXA-B17a	Inclusion fabric in pre-S_m garnet	2539 ± 8	3.0*	600*
10CXA-D102b	Inclusions in pre-S_m garnet	2546 ± 7		
Prograde monazite growth at 1.86 Ga				
10CXA-D54a	Equant inclusions in garnet; matrix grain	1863 ± 6		
10CXA-D102b	Equant inclusions in garnet	1862 ± 14		
Prograde monazite growth at 1.84 Ga				
10CXA-D54a	Equant inclusions in garnet	1840 ± 4		
10CXA-RB2	Inclusion fabric in syn-S_m garnet	1842 ± 4		
Near-peak P-T, syn-S_m monazite growth at 1.82 Ga				
10CXA-B17a	S_m-parallel matrix grains	1826 ± 6	6.6	585
10CXA-D54a	S_m-parallel matrix grains	1827 ± 4	6.5	740
10CXA-RB2	S_m-parallel matrix grains	1825 ± 6	4.3	660
10CXA-D102b	S_m-parallel matrix grains	1829 ± 7	4.5	610
10CXA-D51c	S_m-parallel matrix grain	1815 ± 9		
86SMA-7108a	S_2-parallel grain and equant matrix grains	1815 ± 8		
Monazite growth at 1.8–1.77 Ga				
10CXA-D102b	(?)Crenulation cleavage	1797 ± 10		
09CXA-D003b	Garnet inclusions; matrix grains	1767 ± 6	4.3	550
09CXA-D43b	S_m-parallel garnet inclusions and matrix grains	1798 ± 6	3.8	575
09CXA-D51c	S_m-parallel and equant matrix grains	1787 ± 7		
* = guesstimated conditions; S_m = main fabric external to porphyroblasts				

Table 2. SHRIMP U-Pb monazite results.

																	Apparent age (Ma)		
Spot	Loc	IP	U (ppm)	Th (ppm)	Th / U	$^{206}Pb^*$ (ppm)	$f(206)^{204}$ (%)	$^{208*}Pb/^{206*}Pb$	±%	$^{204}Pb/^{206}Pb$	±%	$^{207*}Pb/^{235}U$	±%	$^{206*}Pb/^{238}U$	±%	Corr Coeff	$^{207}Pb/^{206}Pb$	±%	Disc. (%)
10CXA-B17a (z10594: lat., long. = 67.81673°N, 82.42632°W)																			
26.1	mat || S_m	613	2607	29953	11.9	726	0.103	3.4	0.34	5.9E-5	23	4.97	1.53	0.3240	1.47	0.964	1821	7	0.8
26.1.2	mat || S_m	613	2550	29088	11.8	685	0.037	3.4	0.36	2.1E-5	58	4.82	1.44	0.3130	1.38	0.956	1826	8	4.4
26.2	mat || S_m	613	2679	29087	11.2	798	0.083	3.3	0.37	4.8E-5	23	5.35	1.44	0.3466	1.37	0.955	1832	8	-5.5
26.2.2	mat || S_m	613	2764	30409	11.4	774	0.082	3.2	0.41	4.7E-5	29	4.98	1.47	0.3259	1.39	0.948	1815	9	-0.3
27.1	mat || S_m	613	2820	26294	9.6	806	0.069	2.7	0.35	4.0E-5	29	5.13	1.41	0.3327	1.36	0.964	1831	7	-1.3
27.1.2	mat || S_m	613	2719	25283	9.6	704	0.102	2.7	0.38	5.9E-5	31	4.65	1.44	0.3015	1.37	0.952	1830	8	8.1
7.1	Grt || S_{int}	613	2348	28965	12.7	990	0.171	3.5	0.32	9.9E-5	17	11.36	1.43	0.4908	1.39	0.972	2537	6	-1.8
7.1.2	Grt || S_{int}	613	2283	28200	12.8	894	0.197	3.5	0.38	1.1E-4	21	10.57	1.66	0.4557	1.61	0.969	2540	7	5.6
7.2	Grt || S_{int}	613	2323	33840	15.1	964	0.313	4.2	0.72	1.8E-4	11	11.31	2.70	0.4834	2.36	0.874	2554	22	0.6
7.2.2	Grt || S_{int}	613	2442	34929	14.8	998	0.055	4.1	1.19	3.2E-5	42	11.11	2.53	0.4757	2.05	0.813	2551	25	2.0
10CXA-D102b (z10593: lat., long. = 67.30823°N, 84.77421°W)																			
2.1	mat || S_m	615	2027	26877	13.7	567	0.137	4.04	0.40	7.9E-5	23	4.91	1.9	0.326	1.84	0.948	1786	11	-2.1
2.1.2	mat || S_m	615	1822	29183	16.5	462	0.025	4.86	1.02	1.5E-5	176	4.51	1.7	0.295	1.57	0.903	1815	14	9.3
2.2	mat || S_m	615	4091	28889	7.3	1172	0.055	2.05	0.51	3.2E-5	28	5.06	1.4	0.333	1.34	0.961	1800	7	-3.5
2.2.2	mat || S_m	615	3914	29830	7.9	1035	-0.002	2.24	1.31	-1.0E-6	2066	4.71	1.5	0.308	1.38	0.938	1815	9	5.3
2.3	mat || S_m	615	4614	36550	8.2	1291	0.033	2.28	0.49	1.9E-5	58	4.94	1.5	0.326	1.38	0.945	1801	9	-1.1
2.3.2	mat || S_m	615	3898	30359	8.0	1063	0.046	2.33	0.47	2.7E-5	32	4.82	1.4	0.317	1.37	0.947	1802	8	1.6
2.4	mat || S_m	615	4934	35440	7.4	1483	0.086	2.13	0.62	5.0E-5	41	5.27	1.6	0.350	1.48	0.921	1787	11	-9.5
2.4.2	mat || S_m	615	5270	37964	7.4	1540	0.037	2.13	0.56	2.1E-5	35	5.10	1.6	0.340	1.54	0.963	1777	8	-7.2
60.1	Grt	613	8054	48870	6.3	3402	0.030	1.7	0.24	1.8E-5	21	11.46	1.32	0.4917	1.31	0.993	2548	3	-1.4
60.1.2	Grt	613	10380	54982	5.5	4188	0.008	1.4	0.34	4.9E-6	39	10.90	1.32	0.4697	1.31	0.993	2540	3	2.8
61.1	Grt	613	8092	47155	6.0	3368	0.039	1.6	0.25	2.3E-5	16	11.29	1.32	0.4845	1.31	0.992	2547	3	-0.0
61.1.2	Grt	613	6734	45259	6.9	2702	0.033	1.9	0.25	1.9E-5	22	10.90	1.33	0.4672	1.32	0.991	2550	3	3.7
94.1	mat || S_m	613	3325	36926	11.5	916	0.052	3.4	0.33	3.0E-5	29	4.93	1.41	0.3206	1.36	0.965	1826	7	2.1
94.1.2	mat || S_m	613	3073	33571	11.3	815	0.095	3.4	0.37	5.5E-5	20	4.74	1.44	0.3088	1.37	0.955	1821	8	5.4
95.1	mat || S_m	613	1837	29463	16.6	521	0.025	4.7	0.37	1.4E-5	79	5.20	1.48	0.3305	1.41	0.949	1865	8	1.5
95.1.2	mat || S_m	613	1815	28727	16.3	466	0.104	4.6	0.49	6.0E-5	43	4.68	1.65	0.2992	1.50	0.911	1855	12	10.3
95.2.2	mat || S_m	613	2191	28365	13.4	618	0.067	4.0	0.39	3.9E-5	45	5.09	1.48	0.3285	1.40	0.940	1839	9	0.5
95.2.3	mat || S_m	613	2129	32013	15.5	574	0.079	4.5	0.41	4.6E-5	36	4.87	1.52	0.3142	1.42	0.935	1838	10	4.8
95.3	mat || S_m; rim	613	3591	32598	9.4	933	0.464	2.7	0.53	2.7E-4	12	4.58	1.58	0.3024	1.42	0.899	1796	13	5.9
95.4	mat || S_m	613	2950	34900	12.2	832	0.110	3.4	0.52	6.3E-5	22	5.05	1.74	0.3282	1.63	0.937	1827	11	-0.2

Table 2. (cont.)

																		Apparent age (Ma)		
Spot	Loc	IP	U (ppm)	Th (ppm)	Th / U	^{206}Pb* (ppm)	f(206)^{204} (%)	^{208*}Pb / ^{206*}Pb	±%	^{204}Pb / ^{206}Pb	±%	^{207*}Pb / ^{235}U	±%	^{206*}Pb / ^{238}U	±%	Corr Coeff	^{207}Pb / ^{206}Pb	±%	Disc. (%)
10CXA-D54a (z10592: lat., long. = 67.45851°N, 81.40096°W)																			
110.1	mat || S_m	613	5148	40606	8.1	1419	0.041	2.3	0.36	2.3E-5	34	4.93	1.39	0.3209	1.35	0.968	1823	6	1.8
110.2	mat || S_m	613	5770	46136	8.3	1579	0.096	2.3	0.71	5.6E-5	20	4.89	1.40	0.3186	1.35	0.964	1820	7	2.3
110.3	mat || S_m	613	5691	43221	7.8	1632	0.073	2.2	0.32	4.2E-5	19	5.16	1.37	0.3338	1.33	0.974	1833	6	-1.5
110.4	mat || S_m; core	613	6216	52610	8.7	1774	0.016	2.4	0.38	9.3E-6	69	5.20	1.39	0.3322	1.34	0.963	1857	7	0.5
110.5	mat || S_m	613	5996	48758	8.4	1783	0.031	2.4	0.40	1.8E-5	51	5.34	1.41	0.3462	1.36	0.960	1831	7	-5.4
110.6	mat || S_m	613	4605	36878	8.3	1321	0.019	2.4	0.30	1.1E-5	44	5.10	1.37	0.3339	1.33	0.968	1814	6	-2.8
12.1	Grt; eq	613	5067	43425	8.9	1475	0.077	2.5	0.37	4.5E-5	23	5.28	1.49	0.3389	1.36	0.912	1848	11	-2.1
12.1.2	Grt; eq	613	4504	42092	9.7	1241	0.043	2.7	0.29	2.5E-5	24	4.98	1.36	0.3208	1.33	0.977	1842	5	3.0
16.1	Grt; zoned	613	1114	74627	69.2	313	0.290	20.3	0.36	1.7E-4	21	4.98	1.68	0.3273	1.50	0.891	1805	14	-1.3
2343.1	mat || S_m	613	4778	41077	8.9	1335	0.043	2.5	0.30	2.5E-5	29	5.00	1.39	0.3253	1.36	0.977	1824	5	0.5
2343.1.2	mat || S_m	613	5798	52576	9.4	1536	0.045	2.6	0.90	2.6E-5	36	4.73	1.49	0.3084	1.41	0.946	1820	9	5.5
2343.2	mat || S_m	613	5533	44140	8.2	1621	0.047	2.3	0.32	2.7E-5	28	5.28	1.37	0.3411	1.33	0.973	1837	6	-3.4
2343.2.2	mat || S_m	613	5959	46811	8.1	1626	0.027	2.2	0.45	1.6E-5	22	4.89	1.39	0.3177	1.34	0.969	1827	6	3.0
53.1	Grt-qtz; eq	613	4063	40956	10.4	1148	0.038	3.0	0.38	2.2E-5	36	5.08	1.43	0.3290	1.37	0.962	1831	7	-0.2
53.1.2	Grt-qtz; eq	613	3278	32862	10.4	891	0.035	3.0	0.34	2.0E-5	36	4.90	1.40	0.3163	1.35	0.965	1837	7	4.1
53.2	Grt-qtz; eq	613	4488	47786	11.0	1306	0.067	3.1	0.35	3.9E-5	21	5.21	1.41	0.3387	1.35	0.963	1824	7	-3.6
53.2.2	Grt-qtz; eq	613	4764	47802	10.4	1314	0.025	2.9	0.42	1.4E-5	26	4.96	1.43	0.3211	1.37	0.957	1833	8	2.3
56.1	Grt; eq	613	3185	43574	14.1	909	0.073	4.1	0.33	4.2E-5	27	5.18	1.42	0.3321	1.37	0.960	1849	7	0.0
653.1	Grt; eq	613	3147	35336	11.6	905	0.079	3.6	1.53	4.6E-5	26	5.27	1.40	0.3348	1.35	0.964	1868	7	0.4
653.1.2	Grt; eq	613	3043	36093	12.3	847	0.108	3.7	0.35	6.2E-5	29	5.04	1.62	0.3239	1.50	0.922	1845	11	2.3
658.1	Grt; eq	613	2994	44480	15.3	853	0.200	4.4	0.48	1.2E-4	16	5.13	1.50	0.3316	1.41	0.939	1837	9	-0.6
658.1.2	Grt; eq	613	2585	36760	14.7	715	0.275	4.7	0.72	1.6E-4	25	4.96	1.99	0.3222	1.72	0.863	1825	18	1.5
677.1	Grt; eq	613	8407	57685	7.1	2429	0.040	2.0	0.31	2.3E-5	20	5.21	1.35	0.3364	1.33	0.986	1837	4	-2.0

Spot name follows the convention y.z; where y = grain number and z = spot number. Multiple analyses in an individual spot are labelled as y.z.z
Loc (monazite textural location): mat = matrix grain; Grt = inclusion in garnet; S_m = aligned with S_m fabric; S_{int} = aligned with Grt inclusion fabric; Grt-qtz = inclusion in quartz within garnet; eq = equant; frac = fractured
Uncertainties reported at 1s (absolute) are calculated by numerical propagation of all known sources of error using Squid version 2.2 data reduction program.
f206^{204} refers to mole fraction of total ^{206}Pb that is due to common Pb, calculated using the ^{204}Pb-method;
common Pb composition used is the surface blank (4/6: 0.05770; 7/6: 0.89500; 8/6: 2.13840)
* refers to radiogenic Pb (corrected for common Pb); Disc. = 100 * [1 - ((^{206}Pb/^{238}U age)/(^{207}Pb/^{206}Pb age))]
Calibration reference material = GSC monazite 8153; Age = 512 Ma; ^{206}Pb/^{238}U = 0.0827; U concentration = 2065 ppm
Analytical details:
IP613, 615: 12 µm spot, 5 scans; error in ^{206}Pb/^{238}U calibration = 1.23% and 1.28%.
IP554: 15 µm spot, 5 scans; error in ^{206}Pb/^{238}U calibration = 1.0%. An instrumental mass fractionation correction of 1.007 ± 0.002% was applied to calculated weighted mean ^{207}Pb/^{206}Pb ages based on replicate analyses of monazites 3345 and 2908.

Table 2. (cont.)

																	Apparent age (Ma)		
Spot	Loc	IP	U (ppm)	Th (ppm)	Th / U	$^{206}Pb^*$ (ppm)	$f(206)^{204}$ (%)	$^{208*}Pb/^{206*}Pb$	±%	$^{204}Pb/^{206}Pb$	±%	$^{207*}Pb/^{235}U$	±%	$^{206*}Pb/^{238}U$	±%	Corr Coeff	$^{207}Pb/^{206}Pb$	±%	Disc. (%)
10CXA-D54a (z10592: lat., long. = 67.45851°N, 81.40096°W) (cont.)																			
681.1	mat || S_m	613	2971	53497	18.6	882	0.035	5.4	0.34	2.0E-5	36	5.45	1.45	0.3456	1.39	0.957	1869	8	-2.8
681.1.2	mat || S_m	613	2830	51092	18.7	775	0.087	5.3	0.36	5.0E-5	23	5.01	1.65	0.3190	1.40	0.848	1861	16	4.7
681.2	mat || S_m	613	4122	81375	20.4	1266	0.052	5.8	0.32	3.0E-5	31	5.62	1.43	0.3576	1.37	0.959	1864	7	-6.6
681.2.2	mat || S_m	613	3348	61221	18.9	964	0.051	5.6	0.29	2.9E-5	56	5.25	1.41	0.3353	1.35	0.957	1857	7	-0.5
718.1	Grt; eq	613	3272	36707	11.6	958	0.132	3.5	0.65	7.6E-5	19	5.28	1.43	0.3407	1.37	0.956	1840	8	-3.2
718.1.2	Grt; eq	613	3548	29284	8.5	1010	0.073	2.8	0.57	4.2E-5	21	5.10	1.38	0.3313	1.33	0.969	1828	6	-1.0
10CXA-RB2a, b (z10595: lat., long. = 66.91902°N, 84.21358°W)																			
54.3	mat || S_m	613	10628	58684	5.7	3010	0.151	1.7	0.42	8.7E-5	31	5.04	1.42	0.3297	1.34	0.946	1815	8	-1.4
54.1	mat || S_m	613	10663	59927	5.8	3063	0.014	1.7	0.26	8.1E-6	44	5.12	1.32	0.3344	1.31	0.988	1818	4	-2.6
54.2	mat || S_m	613	11873	67363	5.9	3308	0.011	1.7	0.50	6.4E-6	21	4.97	1.43	0.3243	1.38	0.962	1819	7	0.5
36.1	mat || S_m rim	613	11275	65153	6.0	3246	0.065	1.7	0.54	3.7E-5	26	5.14	1.47	0.3352	1.41	0.956	1820	8	-2.8
54.4	mat || S_m	613	11266	64011	5.9	3196	0.018	1.7	0.34	1.0E-5	41	5.08	1.35	0.3303	1.32	0.980	1823	5	-1.0
122.1	Grt || S_{int}; frac	613	5575	58495	10.8	1611	0.052	3.1	0.31	3.0E-5	26	5.18	1.39	0.3363	1.35	0.971	1828	6	-2.5
72.2.2	Grt || S_{int} core	613	2526	43364	17.7	712	0.068	5.3	0.35	3.9E-5	26	5.06	1.45	0.3282	1.37	0.948	1830	8	0.0
122.1.2	Grt || S_{int}; frac	613	6595	56333	8.8	1854	0.031	2.5	1.07	1.8E-5	36	5.05	1.37	0.3272	1.34	0.976	1831	5	0.4
36.3	mat || S_m core	613	12700	60876	5.0	3749	0.001	1.4	0.42	---	97	5.30	1.38	0.3437	1.34	0.975	1831	6	-4.6
36.2	mat || S_m core	613	11353	66463	6.0	3303	0.030	1.8	0.32	1.7E-5	23	5.23	1.37	0.3387	1.34	0.982	1832	5	-3.0
129.2	Grt || S_{int}	613	3453	65846	19.7	1059	0.097	5.7	0.34	5.6E-5	34	5.52	1.46	0.3571	1.38	0.943	1835	9	-8.5
36.4	mat || S_m core	613	21972	46908	2.2	6268	0.017	0.6	0.65	10.0E-6	31	5.14	1.40	0.3321	1.36	0.969	1835	6	-0.8
122.2	Grt || S_{int}; frac	613	3403	60633	18.4	1015	0.075	5.4	0.39	4.3E-5	23	5.37	1.43	0.3473	1.37	0.958	1836	7	-5.4
72.1.2	Grt || S_{int} core	613	2497	37444	15.5	668	0.059	4.5	0.34	3.4E-5	71	4.82	1.46	0.3112	1.37	0.938	1837	9	5.6
72.1	Grt || S_{int} core	613	2562	39074	15.8	762	0.072	4.5	0.31	4.1E-5	31	5.36	1.43	0.3461	1.37	0.959	1838	7	-4.9
99.1.2	Grt || S_{int}	613	3584	59193	17.1	1029	0.063	5.0	0.30	3.7E-5	23	5.19	1.40	0.3343	1.35	0.963	1841	7	-1.1
121.1.2	Grt || S_{int}	613	6542	42331	6.7	1892	0.017	2.0	0.69	9.8E-6	51	5.23	1.37	0.3367	1.34	0.976	1842	5	-1.8
121.1	Grt || S_{int}	613	7576	56107	7.7	2159	0.011	2.2	0.38	6.1E-6	70	5.15	1.56	0.3317	1.53	0.977	1843	6	-0.3
1144.1.2	mat || S_m core	613	3942	50137	13.1	1102	0.127	3.7	0.37	7.3E-5	21	5.06	1.46	0.3256	1.39	0.950	1844	8	1.7
72.2	Grt || S_{int} core	613	2977	54757	19.0	906	0.032	5.4	0.48	1.8E-5	23	5.51	1.61	0.3542	1.49	0.925	1846	11	-6.8
129.1	Grt || S_{int}	613	4443	49424	11.5	1246	0.030	3.4	0.35	1.7E-5	45	5.09	1.45	0.3264	1.40	0.966	1849	7	1.7
1144.1	mat || S_m core	613	3293	40807	12.8	928	0.514	3.7	0.54	3.0E-4	14	5.13	2.49	0.3281	2.36	0.949	1854	14	1.5
99.1	Grt || S_{int}	613	4019	68893	17.7	1162	0.040	4.9	0.53	2.3E-5	33	5.26	1.52	0.3367	1.44	0.944	1854	9	-1.0

Table 2. (cont.)

																	Apparent age (Ma)		
Spot	Loc	IP	U (ppm)	Th (ppm)	Th U	^{206}Pb* (ppm)	f(206)^{204} (%)	^{208*}Pb ^{206*}Pb	±%	^{204}Pb ^{206}Pb	±%	^{207*}Pb ^{235}U	±%	^{206*}Pb ^{238}U	±%	Corr Coeff	^{207}Pb ^{206}Pb	±%	Disc. (%)
09CXA-D003b (z10211: lat., long. 68.45263°N, 82.78358°W)																			
131.1	mat || S_m	554	2240	35884	16.5	619	1.10	4.9	0.41	6.3E-4	9	4.82	1.43	0.3215	1.136	0.796	1777	16	-1.1
131.1.2	mat || S_m	554	3015	48212	16.5	774	0.76	5.1	0.36	4.4E-4	8	4.45	1.29	0.2987	1.147	0.887	1768	11	4.7
131.1.3	mat || S_m	554	3457	55148	16.5	897	0.26	5.0	0.38	1.5E-4	18	4.52	1.26	0.3021	1.161	0.919	1776	9	4.2
132.1	mat equant	554	1859	35493	19.7	481	0.16	5.8	0.47	9.4E-5	25	4.51	1.24	0.3014	1.150	0.929	1773	8	4.2
132.1.2	mat equant	554	2285	48721	22.0	585	0.10	6.8	0.35	6.0E-5	32	4.45	1.25	0.2980	1.165	0.935	1773	8	5.2
144.1	Grt || S_m	554	2272	46239	21.0	599	0.17	6.3	0.31	9.8E-5	20	4.54	1.20	0.3069	1.128	0.942	1756	7	1.7
144.1.2	Grt || S_m	554	2596	50528	20.1	652	0.11	5.8	0.65	6.4E-5	35	4.37	1.23	0.2925	1.144	0.931	1774	8	6.7
144.2	Grt || S_m	554	2376	54635	23.7	634	0.19	7.2	0.30	1.1E-4	18	4.64	1.29	0.3105	1.228	0.949	1772	7	1.7
144.2.2	Grt || S_m	554	3286	69642	21.9	868	0.12	6.5	0.32	7.2E-5	23	4.56	1.20	0.3075	1.132	0.944	1760	7	1.8
144.2.3	Grt || S_m	554	4630	86549	19.3	1238	0.16	5.7	0.35	9.3E-5	21	4.61	1.38	0.3113	1.271	0.919	1757	10	0.6
189.1	Grt	554	2366	61188	26.7	633	0.26	8.0	0.28	1.5E-4	14	4.63	1.19	0.3116	1.120	0.940	1762	7	0.8
189.2	Grt	554	2397	59030	25.4	649	0.23	7.6	0.47	1.4E-4	23	4.73	1.28	0.3153	1.160	0.905	1780	10	0.7
189.2.1	Grt	554	2819	71525	26.2	742	0.21	8.0	0.35	1.2E-4	22	4.61	1.29	0.3062	1.179	0.913	1784	10	3.5
190.1	Grt	554	2165	62342	29.8	580	0.25	9.1	0.28	1.5E-4	16	4.65	1.22	0.3120	1.132	0.931	1769	8	1.0
190.1.2	Grt	554	2736	76196	28.8	712	0.25	8.8	0.30	1.4E-4	16	4.46	1.24	0.3028	1.147	0.928	1748	8	2.5
230.1	Grt	554	1971	46173	24.2	517	0.23	7.2	0.32	1.3E-4	20	4.56	1.25	0.3053	1.151	0.922	1773	9	3.1
230.1.2	Grt	554	2318	54247	24.2	594	0.15	7.0	0.60	8.5E-5	25	4.45	1.26	0.2986	1.170	0.929	1769	9	4.8
231.1	mat equant	554	2280	53655	24.3	613	0.30	7.2	0.30	1.8E-4	14	4.65	1.21	0.3130	1.126	0.930	1763	8	0.4
231.1.2	mat equant	554	2563	59799	24.1	654	0.59	7.5	0.32	3.4E-4	13	4.45	1.32	0.2970	1.152	0.870	1776	12	5.6
291.1	mat < S_m	554	1612	34296	22.0	437	1.31	6.8	1.02	7.6E-4	12	4.66	2.39	0.3157	1.942	0.813	1748	25	-1.2
291.1.2	mat < S_m	554	1964	45220	23.8	524	0.20	7.3	0.46	1.2E-4	29	4.68	1.42	0.3107	1.259	0.888	1785	12	2.3
291.1.3	mat < S_m	554	2251	51728	23.7	576	0.21	7.2	0.44	1.2E-4	29	4.43	1.42	0.2979	1.260	0.889	1762	12	4.6
291.1.4	mat < S_m	554	2664	61587	23.9	664	0.12	7.0	0.44	6.9E-5	43	4.34	1.40	0.2903	1.259	0.902	1771	11	7.2
82.1	mat || S_m	554	2543	49767	20.2	687	0.17	6.3	0.29	1.0E-4	16	4.68	1.17	0.3146	1.111	0.950	1765	7	0.1
82.1.2	mat || S_m	554	2846	55112	20.0	714	0.16	6.3	0.32	9.5E-5	22	4.33	1.21	0.2921	1.136	0.936	1757	8	6.0

Spot name follows the convention y.z; where y = grain number and z = spot number. Multiple analyses in an individual spot are labelled as y.z.z
Loc (monazite textural location): mat = matrix grain; Grt = inclusion in garnet; S_m = aligned with S_m fabric; S_{int} = aligned with Grt inclusion fabric; Grt-qtz = inclusion in quartz within garnet; eq = equant; frac = fractured
Uncertainties reported at 1s (absolute) are calculated by numerical propagation of all known sources of error using Squid version 2.2 data reduction program.
f206^{204} refers to mole fraction of total ^{206}Pb that is due to common Pb, calculated using the ^{204}Pb-method;
common Pb composition used is the surface blank (4/6: 0.05770; 7/6: 0.89500; 8/6: 2.13840)
* refers to radiogenic Pb (corrected for common Pb); Disc. = 100 * [1 - ((^{206}Pb/^{238}U age)/(^{207}Pb/^{206}Pb age))]
Calibration reference material = GSC monazite 8153; Age = 512 Ma; ^{206}Pb/^{238}U = 0.0827; U concentration = 2065 ppm
Analytical details:
IP613, 615: 12 µm spot, 5 scans; error in ^{206}Pb/^{238}U calibration = 1.23% and 1.28%.
IP554: 15 µm spot, 5 scans; error in ^{206}Pb/^{238}U calibration = 1.0%. An instrumental mass fractionation correction of 1.007 ± 0.002% was applied to calculated weighted mean ^{207}Pb/^{206}Pb ages based on replicate analyses of monazites 3345 and 2908.

Table 2. (cont.)

																	Apparent age (Ma)		
Spot	Loc	IP	U (ppm)	Th (ppm)	Th U	^{206}Pb* (ppm)	f(206)^{204} (%)	^{208*}Pb ^{206*}Pb	±%	^{204}Pb ^{206}Pb	±%	^{207*}Pb ^{235}U	±%	^{206*}Pb ^{238}U	±%	Corr Coeff	^{207}Pb ^{206}Pb	±%	Disc. (%)
09CXA-D043b (z10212: lat., long. = 68.66855°N, 82.76657°W)																			
106.1	mat || S_m	554	2842	73456	26.7	817	0.17	8.2	0.26	9.7E-5	20	5.07	1.16	0.3346	1.097	0.949	1798	7	-3.5
106.1.2	mat || S_m	554	3186	85162	27.6	890	0.17	8.6	0.27	9.9E-5	17	4.91	1.17	0.3253	1.113	0.949	1792	7	-1.3
107.1	mat || S_m	554	2063	26844	13.4	539	5.14	4.2	1.75	3.0E-3	12	4.58	6.02	0.3043	2.834	0.470	1786	97	4.1
107.2	mat || S_m	554	1757	19869	11.7	429	1.70	3.6	1.53	9.8E-4	14	4.34	3.19	0.2839	2.430	0.763	1814	37	11.2
107.2.2	mat || S_m	554	1810	20662	11.8	441	0.99	3.7	1.48	5.7E-4	21	4.33	2.97	0.2837	2.336	0.788	1811	33	11.1
107.2.3	mat || S_m	554	1746	20373	12.1	423	0.60	3.6	1.53	3.5E-4	30	4.29	2.91	0.2821	2.389	0.821	1806	30	11.3
288.1	Grt || S_m	554	1770	20748	12.1	455	1.03	3.7	1.16	5.9E-4	15	4.60	2.52	0.2994	2.117	0.839	1823	25	7.4
288.1.2	Grt || S_m	554	2660	33205	12.9	704	0.20	3.8	0.46	1.1E-4	22	4.66	1.31	0.3080	1.207	0.923	1795	9	3.6
288.1.3	Grt || S_m	554	2883	36519	13.1	727	0.19	3.9	0.45	1.1E-4	23	4.44	1.31	0.2937	1.210	0.922	1795	9	7.5
288.2	Grt || S_m	554	3182	52859	17.2	891	0.26	5.3	0.35	1.5E-4	14	4.94	1.20	0.3261	1.126	0.938	1797	8	-1.2
288.2.2	Grt || S_m	554	3502	53326	15.7	924	0.16	4.7	0.38	9.5E-5	18	4.66	1.21	0.3070	1.142	0.941	1800	7	4.1
478.1	mat || S_m	554	3427	12634	3.8	891	0.07	1.0	0.55	4.0E-5	35	4.63	1.15	0.3028	1.109	0.960	1812	6	5.9
478.1.2	mat || S_m	554	3994	14999	3.9	984	0.08	1.1	0.57	4.7E-5	29	4.37	1.17	0.2867	1.122	0.958	1809	6	10.2
543.1	mat || S_m	554	2688	27298	10.5	710	0.09	3.0	0.39	5.2E-5	31	4.63	1.19	0.3077	1.127	0.951	1787	7	3.2
543.1.2	mat || S_m	554	2862	30560	11.0	715	0.16	3.2	0.41	9.5E-5	17	4.39	1.21	0.2908	1.145	0.947	1791	7	8.1
706.1	Grt || S_m	554	3663	11647	3.3	902	0.27	1.0	1.25	1.5E-4	22	4.36	1.89	0.2868	1.750	0.926	1805	13	9.9
706.2	Grt || S_m	554	2119	14732	7.2	536	0.28	2.2	1.27	1.6E-4	17	4.47	2.13	0.2942	1.963	0.920	1803	15	7.8
706.3	Grt || S_m	554	4650	17865	4.0	1264	0.10	1.3	0.59	5.9E-5	28	4.76	1.17	0.3165	1.108	0.947	1786	7	0.7
09CXA-D051c (z10213: lat., long. = 68.97404°N, -82.99454°W)																			
130.1	mat || S_m	554	2706	30321	11.6	718	0.10	3.4	0.38	5.6E-5	28	4.71	1.19	0.3088	1.129	0.951	1809	7	4.1
130.1.2	mat || S_m	554	3277	37569	11.8	839	0.06	3.5	0.40	3.7E-5	36	4.56	1.20	0.2981	1.145	0.951	1815	7	7.3
130.1.3	mat || S_m	554	4027	47356	12.1	1045	0.05	3.6	0.43	2.7E-5	60	4.64	1.23	0.3020	1.162	0.944	1821	7	6.6
192.1	mat || S_m	554	2471	29551	12.4	678	0.33	4.0	1.05	1.9E-4	23	4.80	2.00	0.3195	1.812	0.906	1781	15	-0.4
192.2	mat || S_m	554	4601	49136	11.0	1246	0.10	3.3	0.65	6.0E-5	56	4.76	1.18	0.3152	1.076	0.911	1792	9	1.4
192.2.2	mat || S_m	554	6278	59959	9.9	1684	0.07	3.0	0.33	3.9E-5	27	4.70	1.11	0.3122	1.078	0.967	1785	5	1.9
192.2.3	mat || S_m	554	7360	68783	9.7	1955	0.06	3.0	0.36	3.5E-5	30	4.63	1.14	0.3092	1.098	0.963	1777	6	2.3
207.1	equant	554	4572	35143	7.9	1226	0.14	2.4	0.45	8.3E-5	14	4.73	1.16	0.3121	1.130	0.972	1797	5	2.6
207.1.2	equant	554	4955	40558	8.5	1290	0.15	2.5	0.34	8.6E-5	15	4.59	1.12	0.3030	1.082	0.966	1798	5	5.1
208.1	equant	554	4455	42567	9.9	1209	0.11	3.0	0.31	6.1E-5	21	4.75	1.11	0.3158	1.073	0.967	1785	5	0.9
208.1.2	equant	554	4977	45766	9.5	1286	0.13	2.9	0.32	7.6E-5	17	4.50	1.12	0.3007	1.082	0.965	1775	5	4.5
333.1	mat || S_m	554	2906	31889	11.3	769	0.37	3.5	1.04	2.1E-4	19	4.65	1.95	0.3082	1.779	0.912	1788	15	3.2
333.1.2	mat || S_m	554	4114	42403	10.6	1084	0.34	3.3	0.43	2.0E-4	9	4.61	1.14	0.3067	1.091	0.955	1784	6	3.3

Table 2. (cont.)

																		Apparent age (Ma)		
Spot	**Loc**	**IP**	**U (ppm)**	**Th (ppm)**	**Th / U**	**^{206}Pb* (ppm)**	**f(206)^{204} (%)**	**^{208*}Pb / ^{206*}Pb**	**±%**	**^{204}Pb / ^{206}Pb**	**±%**	**^{207*}Pb / ^{235}U**	**±%**	**^{206*}Pb / ^{238}U**	**±%**	**Corr Coeff**	**^{207}Pb / ^{206}Pb**	**±%**	**Disc. (%)**
86SMA-7108a (z10596: lat., long. = 69.52365°N, 84.36179°W)																			
26.1	Grt equant	613	883	14337	16.8	241	0.063	4.8	0.51	3.7E-5	99	4.84	1.73	0.3173	1.54	0.889	1808	14	2.0
26.1.2	Grt equant	613	813	12415	15.8	196	-0.001	4.7	0.75	---	---	4.34	2.03	0.2814	1.73	0.855	1828	19	14.2
48.1	mat - equant	613	1005	41948	43.1	291	0.135	12.5	0.40	7.8E-5	28	5.17	2.30	0.3373	2.01	0.877	1820	20	-3.4
48.2	mat - equant	613	939	33873	37.3	260	0.066	11.2	0.63	3.8E-5	200	4.94	2.23	0.3221	1.76	0.788	1818	25	1.1
48.3	mat - equant	613	971	35495	37.8	279	0.020	11.1	0.45	1.2E-5	193	5.09	1.72	0.3341	1.54	0.894	1808	14	-3.2
48.4	mat - equant	613	1076	46391	44.5	315	0.245	12.9	0.60	1.4E-4	22	5.26	2.53	0.3403	1.99	0.783	1834	29	-3.4
48.4.2	mat - equant	613	1040	44852	44.5	288	0.163	13.1	0.44	9.4E-5	27	4.97	1.72	0.3227	1.53	0.887	1827	14	1.5
52.1	Grt - equant	613	935	34829	38.5	275	0.233	11.1	0.40	1.3E-4	22	5.29	1.69	0.3427	1.52	0.902	1831	13	-4.3
52.2	Grt - equant	613	1001	36229	37.4	285	0.118	11.1	0.44	6.8E-5	53	5.02	1.76	0.3314	1.54	0.877	1798	15	-3.0
52.3	Grt - equant	613	928	24030	26.8	260	0.121	7.5	1.00	7.0E-5	28	5.03	2.63	0.3266	2.18	0.828	1827	27	0.3
56.1	mat || S_m	613	1075	41005	39.4	304	0.295	12.0	0.36	1.7E-4	31	5.01	1.72	0.3296	1.48	0.860	1804	16	-2.1
56.2	mat || S_m	613	1263	51327	42.0	375	0.139	11.9	0.69	8.0E-5	38	5.25	2.23	0.3452	1.89	0.846	1805	22	-6.8
56.3	mat || S_m	613	1339	55146	42.5	393	0.009	12.3	0.40	5.5E-6	376	5.19	1.65	0.3420	1.50	0.906	1799	13	-6.2
56.4	mat || S_m	613	1472	56272	39.5	418	0.084	11.1	0.49	4.8E-5	39	5.05	1.79	0.3307	1.59	0.890	1812	15	-1.9
56.4.2	mat || S_m	613	1623	61316	39.0	454	0.072	11.0	0.44	4.1E-5	37	5.02	1.98	0.3256	1.84	0.930	1829	13	0.8

Spot name follows the convention y.z; where y = grain number and z = spot number. Multiple analyses in an individual spot are labelled as y.z.z
Loc (monazite textural location): mat = matrix grain; Grt = inclusion in garnet; S_m = aligned with S_m fabric; S_{int} = aligned with Grt inclusion fabric; Grt-qtz = inclusion in quartz within garnet; eq = equant; frac = fractured
Uncertainties reported at 1s (absolute) are calculated by numerical propagation of all known sources of error using Squid version 2.2 data reduction program.
f206^{204} refers to mole fraction of total ^{206}Pb that is due to common Pb, calculated using the ^{204}Pb-method;
common Pb composition used is the surface blank (4/6: 0.05770; 7/6: 0.89500; 8/6: 2.13840)
* refers to radiogenic Pb (corrected for common Pb); Disc. = 100 * [1 - ((^{206}Pb/^{238}U age)/(^{207}Pb/^{206}Pb age))]
Calibration reference material = GSC monazite 8153; Age = 512 Ma; ^{206}Pb/^{238}U = 0.0827; U concentration = 2065 ppm
Analytical details:
IP613, 615: 12 µm spot, 5 scans; error in ^{206}Pb/^{238}U calibration = 1.23% and 1.28%.
IP554: 15 µm spot, 5 scans; error in ^{206}Pb/^{238}U calibration = 1.0%. An instrumental mass fractionation correction of 1.007 ± 0.002% was applied to calculated weighted mean ^{207}Pb/^{206}Pb ages based on replicate analyses of monazites 3345 and 2908.

Below, the authors present the geological context, textural relationships, thermobarometric data, and geochronological results for these eight samples, starting with two basement samples on the north flank of the Penrhyn Group, two samples of Penrhyn Group, and three samples from northern Melville Peninsula.

10CXA-B17 (B17)

This well foliated (339°/20°) metapsammitic rock from an Archean basement culmination beneath the Penthyn Group contains sparse garnet porphyroblasts up to 5 mm in diameter that are enveloped by matrix biotite and elongate feldspar and quartz grains. Most garnet porphyroblasts contain a quartz inclusion fabric at a high angle to the main foliation and inclusion-free rims up to 0.3 mm in width (Fig. 3).

A 4 mm diameter garnet porphyroblast has a core that has low CaO (X_{Grs} = 0.054–0.058), uniform Fe/(Fe+Mg) of 0.89, and MnO that decreases from the centre (X_{Sp} = 0.10) outward (0.06), indicative of preserved growth zonation. Rims have higher CaO (X_{Grs} = 0.095), Fe/(Fe+Mg) up to 0.91, and MnO (X_{Sp} = 0.09), the last suggestive of minor late-stage garnet resorption. Rim compositions yield pressure-temperature conditions of 6.6 kbar and 585°C. The outer garnet core, together with the cores of matrix biotite and plagioclase farther away from the garnet, yield 3.0 kbar and 600°C, which may approximate the conditions of early garnet growth.

Monazite 7 is an irregular-shaped, elongate grain comprising part of the quartz-inclusion fabric within a large garnet porphyroblast. Four analyses of two spots yield a weighted mean $^{207}Pb/^{206}Pb$ age of 2539 ± 8 Ma (MSWD = 0.31). Six analyses of three spots on two matrix monazite grains that are elongate parallel to the main foliation yield a weighted mean $^{207}Pb/^{206}Pb$ age of 1826 ± 6 Ma (MSWD = 0.70).

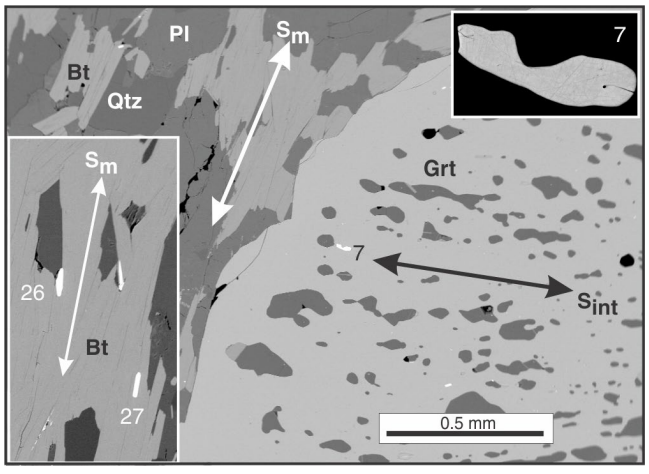

Figure 3. Backscattered electron microscope image of sample B17 showing internal fabric (S_{int}) and monazite (enlarged in upper right inset) within garnet (Grt) porphyroblast. Lower left inset shows two monazite grains aligned with external fabric (S_m). Numbers (7, 26, 27) refer to monazite grains listed in Table 2. Pl = plagioclase, Qtz = quartz, Bt = biotite

10CXA-D102 (D102)

This Archean metapsammitic rock exposed north of the Penrhyn Group displays complex textures. Large, variably resorbed garnet porphyroblasts (0.4–4 mm) contain a well developed quartz-biotite inclusion fabric (Fig. 4) oriented at a moderate to high angle to the matrix foliation (070°/81°) that partly envelops garnet porphyroblasts. Small, subhedral garnet porphyroblasts (<1 mm) preferentially occur in quartz-rich microlithons between which biotite and some sillimanite are aligned subparallel to a variably developed crenulation cleavage that is orthogonal to the main foliation.

The largest garnet porphyroblast has inclusion-free rims up to 0.6 mm in width surrounding its inclusion-rich core; however, the garnet composition is uniform except for slightly higher Fe/(Fe+Mg) at the extreme rim (0.94 versus 0.93 in the core). Rim compositions yield pressure-temperature conditions of 4.5 kbar and 610°C.

A weighted mean $^{207}Pb/^{206}Pb$ age of 2546 ± 7 Ma (MSWD = 2.2) was calculated from four analyses of two monazite inclusions within a large garnet porphyroblast (#60, #61; Fig. 4). One inclusion is elongate parallel to the quartz-biotite fabric within the garnet porphyroblast; the other is equant in shape. Five analyses of two foliation-parallel matrix monazite grains (#94, #95) with moderate Th/U (11.3–15.5) yield an average age of 1829 ± 7 Ma (MSWD = 0.84). A single rim analysis of grain #9 with lower Th/U (#95.3; Th/U = 9.4) was excluded. Duplicate analyses of the visibly indistinct (backscatter electron imaging), higher Th/U (~16.5) core of grain #95 gives a markedly older age of 1862 ± 14 Ma (MSWD = 0.43). Eight

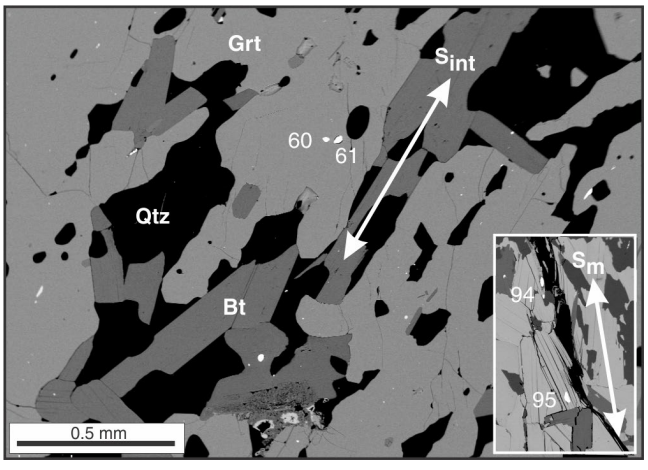

Figure 4. Backscattered electron microscope image of sample D102 showing internal fabric and monazite inclusions (#94, #95) within garnet (Grt) porphyroblast. Inset shows two monazite grains aligned with external fabric (S_m). Qtz = quartz, Bt = biotite

low Th/U (~7.8) analyses of four spots on matrix monazite #2 together with the low Th/U rim analysis #95.3 yield a mean age of 1797 ± 10 Ma (MSWD = 1.90). Monazite #2 is aligned with biotite that has an intermediate orientation between the main foliation and crenulation cleavage.

09CXA-D054 (D54)

This garnet-sillimanite-cordierite metapelite, collected near the eastern edge of exposed Penrhyn Group, is comprised largely of well foliated (296°/84°), biotite-sillimanite-rich bands with variably resorbed, pretectonic garnet porphyroblasts (Fig. 5) that are commonly rimmed by cordierite. Thin, concordant, discontinuous lenses and 1 mm wide band of coarser grained K-feldspar and quartz with scattered, fine-grained biotite are interpreted as crystallized melt.

A 2 mm diameter garnet porphyroblast has a more magnesian (Fe/(Fe+Mg) = 0.75) and calcic (X_{Grs} = 0.042) core than rims (0.81, 0.038, respectively). The rims also have slightly higher MnO, consistent with garnet resorption. Biotite is uniform in composition, suggesting that its large modal abundance was sufficient to prevent significant Fe enrichment during garnet resorption. Plagioclase immediately adjacent to garnet is strongly zoned from more calcic rims (X_{An} = 0.50) to cores (X_{An} = 0.33). Pressure-temperature conditions of 3.0 kbar and 640°C derive from rim compositions of plagioclase in contact with garnet. Near-peak conditions of 6.5 kbar and 740°C are estimated from the intersection within the melt stability field of calculated Fe/(Fe+Mg) and X_{Grs} isopleths that match the garnet core composition (Fig. 6). These results indicate a clockwise pressure-temperature-time path (Fig. 6) during which cordierite grew near the metamorphic peak and/or upon postpeak decompression.

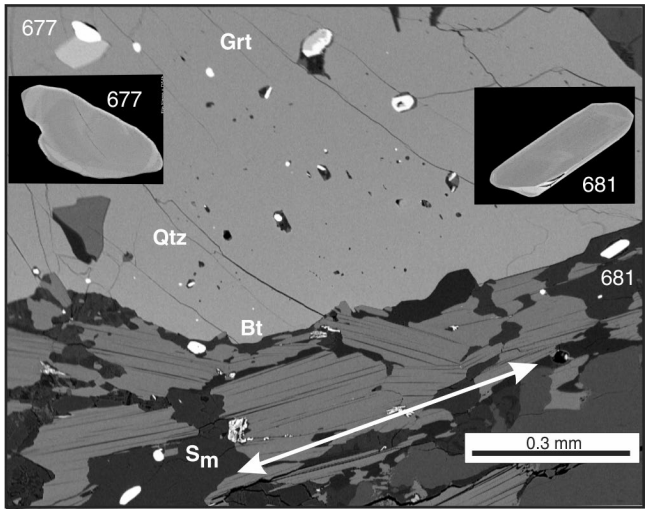

Figure 5. Backscattered electron microscope image of sample D54 showing pretectonic garnet (Grt) without internal fabric and matrix biotite (Bt) (with monazite #681) defining external foliation (S_m). Qtz = quartz

Monazite ages fall into three distinct groups. An average age of 1863 ± 6 Ma (MSWD = 0.55) derives from six analyses of three grains: a small (20 µm wide), elongate, matrix grain parallel to the main foliation (#681; Fig. 5); the core of a large (80 µm wide), foliation-parallel matrix grain (#110) within leucosome; and an equant inclusion in garnet (#653.2). The same age, but with slightly larger errors, results from the four analyses of monazite #681, which has distinctly higher Th and Th/U than most other monazite. The youngest pooled age, 1827 ± 4 Ma (MSWD = 1.3, n = 13), stems from five analyses outside the core of foliation-parallel matrix grain #110, four analyses of matrix grain #2343, and a monazite inclusion inside quartz within garnet (#53). The last textural location has commonly been found to incompletely shield monazite from interaction with metamorphic fluids (R.G. Berman, unpub. data, 2005). An intermediate age of 1840 ± 4 Ma (MSWD = 0.97, n = 10) derives from six monazite inclusions in garnet that are not intersected by fractures or contained within quartz (#12, #56, #653, #658, #677, #718), excluding one older analysis (#653.1).

10CXA-R2 (R2)

This garnet-sillimanite-cordierite metatexite, collected from the western Penrhyn Group near Lyon Inlet (Fig. 2), displays a strong foliation (245°/85°) in biotite-sillimanite-rich layers and very little shape fabric in coarser grained,

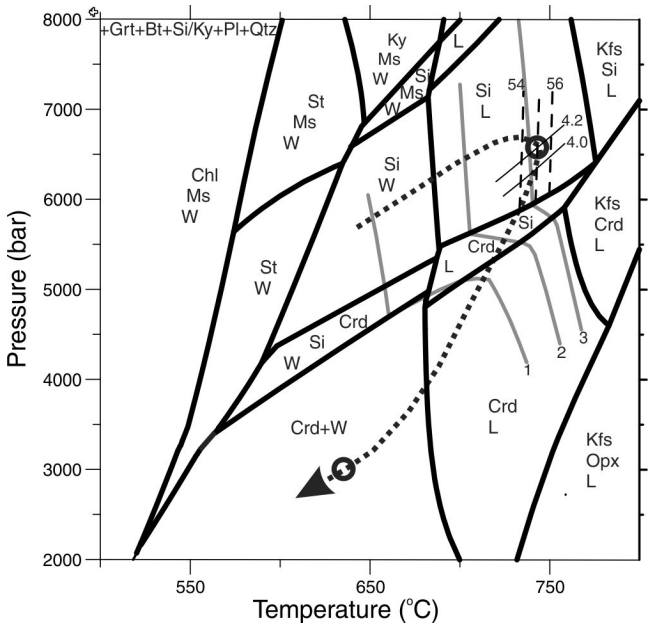

Figure 6. Calculated phase diagram for sample D54, with isopleths (%) of modal garnet (grey solid curves; 1–3%), X_{Grs} (thin solid curves; 4.0, 4.2%), and Fe# (dashed curves; 54–56). Bold circles show thermobarometric (peak and post-peak P-T) results plotted along estimated P-T path (dotted curve). Grt = garnet, Bt = biotite, Si = sillimanite, ky = kyanite, Pl = plagioclase, Qtz = quartz, Ms = muscovite, Chl = chlorite, St = staurolite, Kfs = potassium feldspar, Crd = cordierite, Opx = orthopyroxene, L = melt, W = H_2O. For clarity, some small stability fields are not shown.

concordant K-feldspar-rich layers (leucsosome). Garnet porphyroblasts are strongly resorbed, and many host fine- to medium-grained sillimanite inclusions that outline a distinct internal fabric parallel to the main external foliation (Fig. 7). The elongation of garnet porphyroblasts parallel to the main foliation (Fig. 7) indicates syntectonic growth.

Minimal compositional variations (<1 mol %) occur in matrix plagioclase, biotite, and cordierite, as well as a 0.7 mm diameter garnet porphyroblast that hosts monazite #72 (*see* below). Rim compositions yield pressure-temperature conditions of 4.3 kbar and 660°C.

An almost continuous range of ages between 1854 Ma and 1815 Ma, which do not form a single statistical population (MSWD = 2.5), were obtained from large (>100 µm diameter) matrix grains (#36, #54) within coarse-grained leucosome and from much smaller (<20 µm diameter) grains consisting of a matrix monazite (#1144) and monazite inclusions in garnet porphyroblasts hosting a sillimanite-inclusion fabric. A weighted mean age of 1825 ± 6 Ma (MSWD = 1.7) derives from eight analyses of two large matrix monazite grains (#36, #54) that are elongate parallel to the main foliation and both associated with leucosome. A weighted mean age of 1842 ± 4 Ma (MSWD = 0.63, n = 12) derives from all monazite inclusions in garnet that are not visibly intersected by fractures (Table 2; Fig. 7) and one small matrix grain (#1144) within a biotite-rich layer. Including analyses of garnet inclusions intersected by fractures in addition to those of the core of matrix grain #36 gives a slightly younger mean age of 1837 ± 3 Ma (MSWD = 1.05).

09CXA-D003 (D3)

This garnet-biotite-muscovite metapsammite, collected from the southern part of a package of Archean metavolcanic and metasedimentary rocks forming the Roche Bay belt (Fig. 2), has a well developed foliation (044°/77°) defined by aligned biotite and rare muscovite grains. Euhedral, post-tectonic garnet porphyroblasts up to 1 mm in diameter host foliation-parallel quartz inclusions and crosscut matrix biotite (Fig. 8). A 2 mm diameter garnet porphyroblast uniform Fe/(Fe+Mg), X_{Grs} (0.050–0.055). The X_{Sps} decreases from core (X_{Sps} = 0.07) to rim (X_{Sps} = 0.02), consistent with preserved growth zoning. Rim compositions yield pressure-temperature conditions of 4.3 kbar and 550°C.

Twenty-five SHRIMP analyses of nine monazite grains range between 1772 Ma and 1735 Ma and yield a weighted mean $^{207}Pb/^{206}Pb$ age of 1767 ± 6 Ma (MSWD = 1.02). The monazite grains range in size from 15 µm to 25 µm wide and 20 µm to 70 µm long. They show a range of textural settings (Table 2), including matrix grains and a garnet inclusion aligned parallel to the main foliation, equant matrix grains or garnet inclusions, and one matrix grain at a high angle to the foliation.

09CXA-D043 (D43)

This Archean metapsammite from the central portion of Roche Bay belt (Fig. 2) displays a strong, north-striking, steep foliation defined by aligned biotite and elongate porphyroblasts of garnet and matrix quartz and feldspar. This fabric is weakly crenulated, except adjacent to some rotated garnet porphyroblasts. Garnet porphyroblasts are interpreted as syntectonic with respect to the main foliation, as they are elongate and contain a weak to moderate internal fabric parallel to the main foliation (Fig. 9).

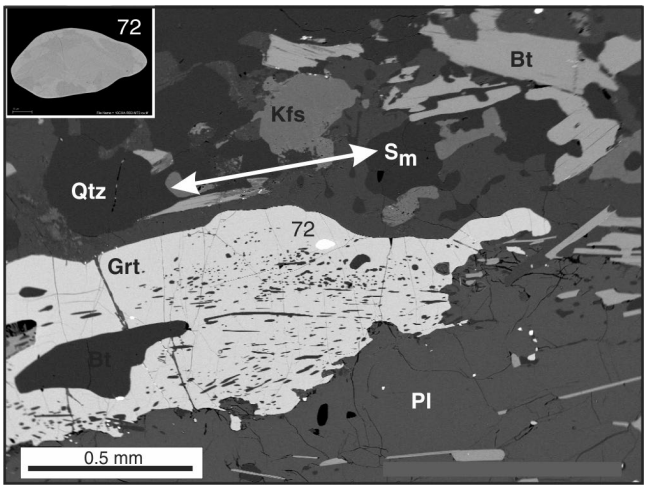

Figure 7. Backscattered electron microscope image of sample R2 showing elongate garnet (Grt) porphyroblast hosting sillimanite inclusions and monazite #72. Qtz = quartz, Kfs = potassium feldspar, Bt = biotite, Pl = plagioclase, S_m = external fabric

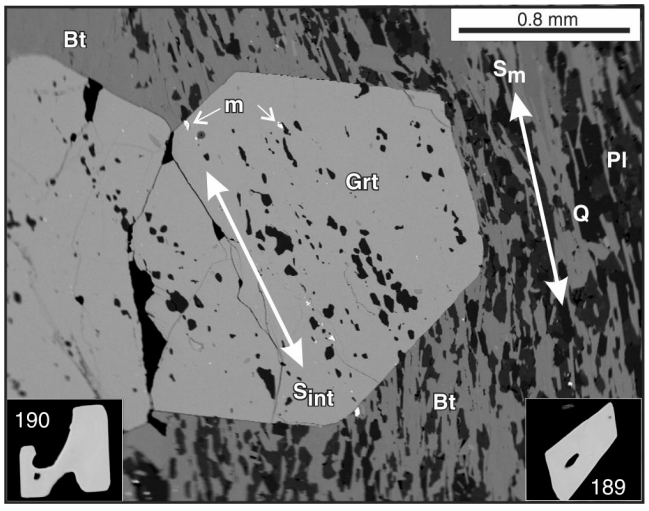

Figure 8. Backscattered electron microscope image showing post-tectonic garnet (Grt) in sample D3 with two monazite inclusions (m) that were not analyzed because of their small size (<10 µm). Insets show analyzed monazite inclusions (#189, #190) that are randomly oriented in a different garnet porphyroblast. Bt = biotite, Pl = plagioclase, Q = quartz, S_{int} = internal fabric, S_m = external fabric

A 1.7 mm diameter garnet porphyroblast has uniform Fe/(Fe+Mg) and X_{Grs} (0.035–0.041). The X_{Sps} decreases from core (X_{Sps} = 0.03) to rim (X_{Sps} = 0.01), indicating some growth zoning is preserved. Matrix plagioclase varies from $An_{29–30}$ more than 400 µm from garnet to $An_{19–21}$ adjacent to and touching garnet. The latter yield pressure-temperature conditions of 3.8 kbar and 575°C.

Eighteen SHRIMP analyses of six monazite grains range between 1811 Ma and 1773 Ma and yield a weighted mean $^{207}Pb/^{206}Pb$ age of 1798 ± 6 Ma (MSWD = 1.13). The monazite grains are all aligned parallel to the foliation, either in the matrix or as inclusions in garnet (e.g. Fig. 9).

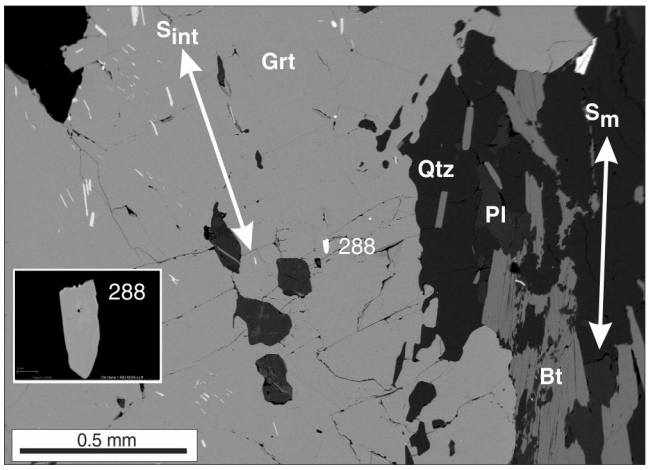

Figure 9. Backscattered electron microscope image of sample D43 showing garnet (Grt) porphyroblast with internal fabric (S_{int}) and monazite (#288) aligned subparallel to external foliation (S_m). Qtz = quartz, Pl = plagioclase, Bt = biotite

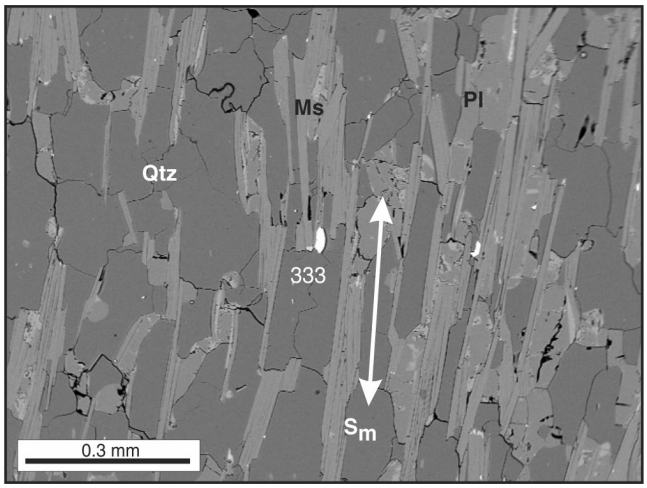

Figure 10. Backscattered electron microscope image of sample D51 showing matrix monazite #333 aligned with foliation defined by muscovite (Ms) and the shape fabric of quartz (Qtz). Pl = plagioclase, S_m = external fabric

09CXA-D051 (D51)

This Archean muscovite-biotite metapsammite is part of a supracrustal assemblage that includes banded iron-formation, conglomerate, and volcanoclastic rocks at the northern end of the Roche Bay belt (Fig. 2). A well developed foliation (150°/55°) is defined by scattered grains of poikioblastic biotite aligned with fine-grained muscovite (Fig. 10). Due to the absence of garnet, pressure-temperature constraints were not obtained.

Thirteen SHRIMP analyses of five monazite grains range between 1821 Ma and 1775 Ma, but do not form a statistical population (MSWD = 4.9). A weighted mean $^{207}Pb/^{206}Pb$ age of 1815 ± 9 Ma (MSWD = 0.77) derives from three analyses of a 15 µm × 30 µm matrix monazite (#130) that is parallel to the foliation. The other analyses, also of matrix monazite, yield a mean age of 1787 ± 7 Ma (MSWD = 1.89). Two of these grains are elongate parallel to the main foliation (Fig. 10) and two are equant grains. Whereas most grains lie on grain boundaries or within plagioclase intersected by fractures (#192), monazite #130 is included almost entirely within unfractured matrix plagioclase, apparently armouring it from later reaction or recrystallization.

86SMA-7108 (7108)

This garnet-biotite metapsammite, taken from the GSC's archival collection, was collected from a weakly gneissic rock in the northern granulite block (Fig. 2). In thin section, it displays two distinct fabrics at a high angle to one another (Fig. 11). The S_1 fabric is defined by the flattening of quartz, plagioclase, and K-feldspar. A moderate S_2 cleavage is defined by aligned biotite and reorientation of some

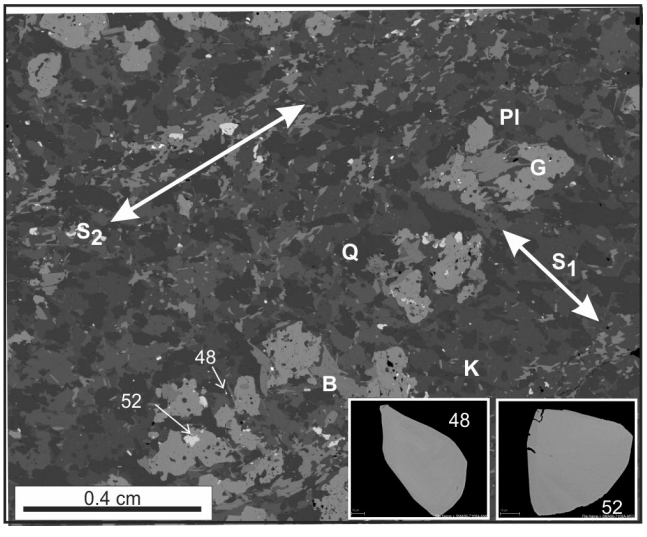

Figure 11. Backscattered electron microscope image of sample 7108 showing two distinct fabrics (S_1, S_2) and location of two analyzed monazite grains: #48 is aligned in the earlier (S_1) fabric; #52 is an equant inclusion in garnet (G). Qtz = quartz, Pl = plagioclase, B = biotite, K = K-feldspar

quartz grains. Anhedral, embayed garnet porphyroblasts are post-tectonic, overgrowing the S_1 fabric (Fig. 11), and in several instances cutting S_2-parallel biotite. A 1.5 mm diameter garnet porphyroblast shows slight zoning, with X_{Grs} decreasing by 0.02 and Fe/(Fe+Mg) increasing by 0.01 from core to rim. Dispersed biotite grains have about 0.04 lower Fe/(Fe+Mg) further from garnet, suggesting that more proximal biotite was enriched in FeO during garnet resorption; however, garnet rims do not show the MnO enrichment that typically accompanies this process (Kohn and Spear, 2000). For this reason, pressure-temperature conditions (4.5 kbar and 675°C) calculated from the lowest Fe/(Fe+Mg) biotite are considered unreliable.

Fifteen analyses of four monazite grains yield a weighted mean age of 1815 ± 8 Ma (MSWD = 0.61). One of these grains (#56) is an elongate inclusion in biotite parallel to the S_2 fabric, whereas the rest are subequant in shape (e.g. Fig. 11).

DISCUSSION

The quantitative metamorphic and geochronological data presented above provide first-order constraints on the tectonometamorphic evolution of Melville Peninsula, with the data constraining two distinct metamorphic and deformational events.

Neoarchean tectonometamorphic event at 2.54 Ga

Two widely separated samples, B17 and D102 (Fig. 2), contain monazite inclusions in garnet with pooled ages of 2539 ± 8 Ma and 2546 ± 7 Ma, respectively. Two of three of these monazite grains are elongate parallel to the distinct internal fabric within garnet porphyroblasts, suggesting that they date an early, amphibolite-facies deformation event. This event is provisionally attributed to the early stages of development of the ca. 2.54–2.3 Ga Arrowsmith Orogen (Berman et al., 2005; 2013a; Hartlaub et al., 2007; Schultz et al., 2007). Textural relationships pointing to deformation near the beginning of this time period support the suggestion based on U-Pb zircon data on Boothia Peninsula that this event initiated in a convergent setting by ca. 2.54 Ga (Berman et al., 2013a).

Paleoproterozoic tectonometamorphic event

The four samples from southern Melville Peninsula (two of the Penrhyn Group; two of basement on its north flank) preserve a record of monazite growth between ca. 1860 Ma and 1820 Ma, documenting a major tectonometamorphic event affecting this region. Two samples (D54, D102) record evidence that metamorphism initiated by 1863 ± 6 Ma. The equant shape of most of the monazite grains in this ca. 1863 Ma population (except one matrix grain in sample D54) suggest that strong regional deformation initiated after this time. Samples D54 and R2 record ca. 1840 Ma monazite growth, with the occurrence in R2 of 1842 Ma monazite as foliation-parallel inclusions in garnet pointing to syntectonic garnet growth. Matrix monazite ages between 1829 ± 4 Ma and 1825 ± 4 Ma in four samples of, and adjacent to the Penrhyn Group are interpreted to date peak metamorphism because of the association of this monazite with leucosome in two samples (R2, D54). The occurrence of all of these ca. 1827 Ma monazite grains as elongate crystals parallel to the main foliation is consistent with syntectonic crystallization. The earlier deformation recorded by sample R2 proximal to the Lyon Inlet boundary zone suggests that this structure may have been active at ca. 1842 Ma, consistent with metamorphic zircon growth at this time in a Neoarchean granodiorite in this boundary zone (Ganderton, 2013).

The above age results accord well with those obtained by electron microprobe dating of monazite from several locations in the central and eastern parts of the Pehnryn Group (Lillydahl-Schroeder, 2013). Lillydahl-Shroeder (2013) pooled results from several widely separated samples to interpret ca. 1853 ± 5 Ma monazite growth prior to significant garnet crystallization, garnet growth at ca. 1839 ± 8 Ma, peak metamorphism and melting at 1819 ± 6 Ma, and retrograde metamorphism at 1794–1776 Ma. Deformation at single locations was interpreted to have been dated at 1853 ± 9 Ma (top to the south shearing), 1845 ± 9 Ma (microfolding), and 1823 ± 22 Ma (folding).

The present study documents four samples (7108, D51, D43, D3) from northern Melville Peninsula (Prince Albert and northern granulite blocks) that record somewhat (ca. 1815 Ma) to significantly (ca. 1798–1767 Ma) younger monazite ages than samples further south on Melville Peninsula (Fig. 2). Textural relationships do not indicate whether these ages relate to prograde or near-peak metamorphism. In contrast to the other three samples (7108, D51, D3), all of the monazite grains in D43 occur as elongate grains parallel to the main foliation, consistent with syntectonic crystallization at 1798 ± 4 Ma. This textural difference may relate to the location of D43 in the north-striking portion of the horseshoe-shaped Roche Bay belt (Fig. 2). If so, the deformation recorded in this sample may reflect the onset of east-west compression that affected much of the central Rae Craton (Berman et al., 2005, 2008, 2010a), and was dated at ca. 1790 Ma in the Committee Bay region (Berman et al., 2010a).

Petrological calculations for Penrhyn Group sample D54 define a clockwise P-T-t path characteristic of crustal thickening driving regional metamorphism. This conclusion is supported by the absence of Paleoproterozoic plutonic rocks that could have provided a premetamorphic heat source, as no plutonic rocks have been identified regionally between ca. 2.02 Ga (Wodicka, 2011; monzogranite) and 1.83 Ga (S. Erdman, unpub. data, 2011; monzogranite). Post-tectonic monzogranite intruded Penrhyn Group rocks at 1816 ± 4 Ma to 1812 ± 3 Ma (Erdmann et al., 2013), consistent with an

origin via crustal melting subsequent to thermal incubation of the middle crust. The approximately 2 kbar higher pressure recorded by garnet rims in sample B17 compared to D54 (Fig. 2) may reflect the location of B17 in an overthrust basement nappe. Samples farther north record very similar pressures at slightly lower temperatures compared to Penrhyn Group samples.

The ca. 1860–1790 Ma monazite ages determined in this study are remarkably similar to those determined in adjacent regions (Fig. 1) in the Committee Bay belt to the west (Berman et al., 2005, 2010a) and on Southampton Island to the south (Berman et al., 2013b). Together these data provide a consistent time window for northwest-vergent deformation and metamorphism of the central Rae Craton, which Berman et al. (2010b) modelled to result from ca. 1870 Ma collision of the southeastern flank of the Rae Craton with Meta Incognita microcontinent (St-Onge et al., 2006).

ACKNOWLEDGMENTS

This project was funded by the GSC's Northern Mineral Resources and Development Program, the Canada-Nunavut Geoscience Office, and Polar Continental Shelf Program. The authors thank P. Hunt, T. Pestaj, and K. Venance for assistance with acquiring SEM, SHRIMP, and microprobe data, respectively. A constructive review of this paper by S. Pehrsson is greatly appreciated.

REFERENCES

Berman, R.G., 2007. winTWQ (version 2.3): A Microsoft Windows-compatible software package for performing internally-consistent thermobarometric calculations; Geological Survey of Canada, Open File 5462. doi:10.4095/223425

Berman, R.G., 2010. Metamorphic map of the western Churchill Province; Geological Survey of Canada, Open File 5279, 3 sheets, 55 p. doi:10.4095/287320

Berman, R.G., Sanborn-Barrie, M., Stern, R.A., and Carson, C.J., 2005. Tectonometamorphism at ca. 2.35 and 1.85 Ga in the Rae Domain, western Churchill Province, Nunavut, Canada; insights from structural, metamorphic and *in situ* geochronological analysis of the southwestern Committee Bay Belt; Canadian Mineralogist, v. 43, p. 409–442. doi:10.2113/gscanmin.43.1.409

Berman, R.G., Ryan, J.J., Davis, W.J., and Nadeau, L., 2008. Preliminary results of linked in-situ SHRIMP dating and thermobarometry studies in the Boothia mainland area, north-central Rae Province, Nunavut; Geological Survey of Canada, Current Research 2008-2, 13 p. doi:10.4095/224805

Berman, R.G., Sanborn-Barrie, M., Rayner, N., Carson, C., Sandeman, H., and Skulski, T., 2010a. Petrological and in situ SHRIMP geochronological constraints on tectonometamorphic evolution of the Committee Bay belt, Nunavut; Precambrian Research, v. 181, p. 1–20. doi:10.1016/j.precamres.2010.05.009

Berman, R.G., Sandeman, H.A.I., and Camacho, A., 2010b. Diachronous deformation and metamorphism in the Committee Bay belt, Rae Province, Nunavut: insights from ^{40}Ar-^{39}Ar cooling ages and thermal modelling; Journal of Metamorphic Geology, v. 28, p. 439–457. doi:10.1111/j.1525-1314.2010.00873.x

Berman, R.G., Pehrsson, S., Davis, W.J., Ryan, J., Qiu, H., and Ashton, K.E., 2013a. The Arrowsmith orogeny: new insights from in situ SHRIMP geochronology of the southwestern and central Rae craton; Precambrian Research, v. 232, p. 44–69. doi:10.1016/j.precamres.2012.10.015

Berman, R.G., Rayner, N., Sanborn-Barrie, M., and Whalen, J., 2013b. The tectonometamorphic evolution of Southampton Island, Nunavut: insight from petrologic modeling and in situ SHRIMP geochronology of multiple episodes of monazite growth; Precambrian Research, v. 232, p. 140–166. doi:10.1016/j.precamres.2012.08.011

Corrigan, D., Nadeau, L., Brouillette, P., Wodicka, N., Houle, M., Tremblay, T., Machado, G., and Keating, P., 2013. Overview of the Melville Peninsula GEM-Mineral geoscience project; Geological Survey of Canada, Current Research 2013-19, 21 p. doi:10.4095/292862

Erdmann, S., Wodicka, N., Jackson, S.E., and Corrigan, D., 2013. Zircon textures and composition; refractory recorders of magmatic volatile evolution?; Contributions to Mineralogy and Petrology, v. 165, p. 45–71. doi:10.1007/s00410-012-0791-z

Ganderton, N., 2013. Mapping and zircon geochronology of the Lyon Inlet boundary zone, Nunavut: a crustal-scale break in the Churchill Province; M.Sc. thesis, University of Western Ontario, London, Ontario, 87 p.

Hartlaub, R.P., Heaman, L.M., Chacko, T., and Ashton, K.E., 2007. Circa 2.3 Ga magmatism of the Arrowsmith Orogeny, Uranium City region, western Churchill Craton, Canada; The Journal of Geology, v. 115, p. 181–195. doi:10.1086/510641

Henderson, J.R., 1983. Structure and metamorphism of the Aphebian Penrhyn Group and its Archean basement complex in the Lyon Inlet area, Melville Peninsula, District of Franklin; Geological Survey of Canada, Bulletin 324, 50 p. doi:10.4095/119500

Kohn, M.J. and Spear, F., 2000. Retrograde net transfer reaction insurance for pressure-temperature estimates; Geology, v. 28, p. 1127–1130. doi:10.1130/0091-7613(2000)28<1127:RNTRIF>2.0.CO;2

Lillydahl-Schroeder, H., 2013. New petrological and in situ electron microprobe monazite age constraints on the timing of the Foxe Orogeny, Melville Peninsula, Nunavut, Canada; M.Sc. thesis, Boston College, Boston, Massachusetts, 209 p.

Rayner, N. and Stern, R.A., 2002. Improved sample preparation method for SHRIMP analysis of delicate mineral grains exposed in thin sections; Geological Survey of Canada, Current Research 2002-F10, 3 p. doi:10.4095/213626

Schultz, M., Chacko, T., Heaman, L.M., Sandeman, H., Simonetti, A., and Creaser, R.A., 2007. The Queen Maud Block: A newly recognized Paleoproterozoic (2.4–2.5 Ga) terrane in northwest Laurentia; Geology, v. 35, p. 707–710. doi:10.1130/G23629A.1

Spratt, J.E., Jones, A.G., Hogg, C., and Corrigan, D., 2013. Lithospheric geometry revealed by deep-probing magneto-telluric surveying, Melville Peninsula, Nunavut; Geological Survey of Canada, Current Research 2013-12, 18 p. doi:10.4095/292482

St-Onge, M.R., Wodicka, N., and Ijewliw, O., 2006. Polymetamorphic evolution of the Trans-Hudson Orogen, Baffin Island, Canada: integration of petrological, structural and geochronological data; Journal of Petrology, v. 48, p. 271–302. doi:10.1093/petrology/egl060

Stern, R.A., 1997. The GSC Sensitive High Resolution Ion Microprobe (SHRIMP): analytical techniques of zircon U-Th-Pb age determinations and performance evaluation; Geological Survey of Canada, Current Research 1997-F, 31 p. doi:10.4095/209089

Stern, R.A. and Berman, R.G., 2001. Monazite U-Pb and Th-Pb geochronology by ion microprobe, with an application to in situ dating of an Archean metasedimentary rock; Chemical Geology, v. 172, p. 113–130. doi:10.1016/S0009-2541(00)00239-4

Wodicka, N., Corrigan, D., Nadeau, L., and Erdmann, S., 2011. New U-Pb geochronological results from Melville Peninsula: unravelling the Archean and early Paleoproterozoic magmatic history of the north-central Rae craton; Geological Association of Canada–Mineralogical Association of Canada Abstracts, v. 34, p. 236.

Geological Survey of Canada Project 340523NU62